Structure, Vol. 13, 55–63, January, 2005, ©2005 Elsevier Ltd All rights reserved. DOI 10.1016/j.str.2004.10.016

A Structural Pathway for Signaling in the E46Q Mutant of Photoactive Yellow Protein

Sudarshan Rajagopal,[1] Spencer Anderson,[2] Vukica Srajer,[2] Marius Schmidt,[4] Reinhard Pahl,[2] and Keith Moffat[1,2,3,*]
[1]Department of Biochemistry and Molecular Biology
[2]Center for Advanced Radiation Sources
[3]Institute for Biophysical Dynamics
University of Chicago
920 East 58th Street
Chicago, Illinois 60637
[4]Physik-Department E17
Technische Universitaet Munchen
Garching, 85748
Germany

Summary

In the bacterial photoreceptor photoactive yellow protein (PYP), absorption of blue light by its chromophore leads to a conformational change in the protein associated with differential signaling activity, as it executes a reversible photocycle. Time-resolved Laue crystallography allows structural snapshots (as short as 150 ps) of high crystallographic resolution (1.6 Å) to be taken of a protein as it functions. Here, we analyze by singular value decomposition a comprehensive time-resolved crystallographic data set of the E46Q mutant of PYP throughout the photocycle spanning 10 ns–100 ms. We identify and refine the structures of five distinct intermediates and provide a plausible chemical kinetic mechanism for their interconversion. A clear structural progression is visible in these intermediates, in which a signal generated at the chromophore propagates through a distinct structural pathway of conserved residues and results in structural changes near the N terminus, over 20 Å distant from the chromophore.

Introduction

Understanding the structural bases for regulation and signaling in proteins is a central problem in biophysics (Lim, 2002). What are the active and inactive conformations of a protein? How does a protein traverse a complex energy landscape as it passes from one conformational state or substate to another (Frauenfelder et al., 2001)? Answers to these questions require the structures of all intermediates and the rates by which they interconvert, i.e., the chemical kinetic mechanism. They also require identification of those residues responsible for relaying the structural signal from one part of the protein to the next, i.e., the structural pathway for energy transduction.

In a photoreceptor, the primary event of photon absorption by its chromophore results in a local structural signal that is then relayed to and through the surrounding protein, resulting in conformational changes associated with differential activity (Hellingwerf, 2002). Photoactive yellow protein (PYP) is a blue light photoreceptor that is thought to regulate a negative phototactic response in *Halorhodospira halophila* (Sprenger et al., 1993). In PYP, absorption of a photon initiates a reversible photocycle characterized by *trans-cis* isomerization of its 4-hydroxycinnamic acid chromophore and the adoption of a "signaling state" by the surrounding protein in milliseconds (Hoff et al., 1999). PYP is a member of the PAS domain superfamily, whose members are present in all kingdoms of life. Sensor PAS domains are capable of binding a wide variety of ligands that regulate their signaling activity, such as small organics, flavins, and heme (Taylor and Zhulin, 1999). Structural changes induced in the PAS domain by the ligand in turn control cellular processes through interactions with a wide variety of cognate effector domains, such as phosphodiesterases, histidine kinases, and serine/threonine kinases (Crosson et al., 2003; Taylor and Zhulin, 1999). Studies of PYP, therefore, examine signaling mechanisms that may be relevant to the entire PAS domain superfamily.

Because of its favorable spectroscopic properties and high solubility, the photocycle of PYP and the intermediates that populate it have been probed by a variety of biophysical methods such as NMR, conventional and time-resolved crystallography, FT-IR, and visible absorption spectroscopy (reviewed by Hellingwerf et al., 2003; Cusanovich and Meyer, 2003). Time-resolved Laue crystallography allows both short time resolution, as low as 150 ps (Schotte et al., 2003), and complete structural detail to relatively high crystallographic resolution (~1.6 Å) (Ren et al., 1999). Interpretation of the structural and temporal information present in time-resolved crystallographic data requires a method for deconvolution of the difference electron density arising from the different intermediates that populate the same time range (Schlichting and Chu, 2000). Singular value decomposition (SVD) allows for a complete analysis of the structural and temporal components of the data (Henry and Hofrichter, 1992; Schmidt et al., 2003). Schmidt and coworkers (Schmidt et al., 2004) recently applied SVD to time-resolved crystallographic data spanning the later stages of the photocycle of wild-type (WT) PYP from microseconds to milliseconds. They determined the structures of two late intermediates and identified the mechanism for the late time range of the photocycle (Schmidt et al., 2004).

Recently, the most comprehensive time-resolved Laue data on any protein were obtained. These data consist of 30 time points, measured from nanoseconds to milliseconds, throughout the photocycle of the E46Q mutant of PYP (E46Q PYP) (Anderson et al., 2004b). In solution, this mutant undergoes a photocycle qualitatively similar to that of WT PYP but roughly 60 times faster (Genick et al., 1997b), although the nature of the structural changes in these states is different due to the lack of charge on residue 46 in E46Q (Xie et al., 2001). By separating the Laue data into early (10–500 ns) and late (10 μs–24 ms) time ranges, followed by averaging

*Correspondence: moffat@cars.uchicago.edu

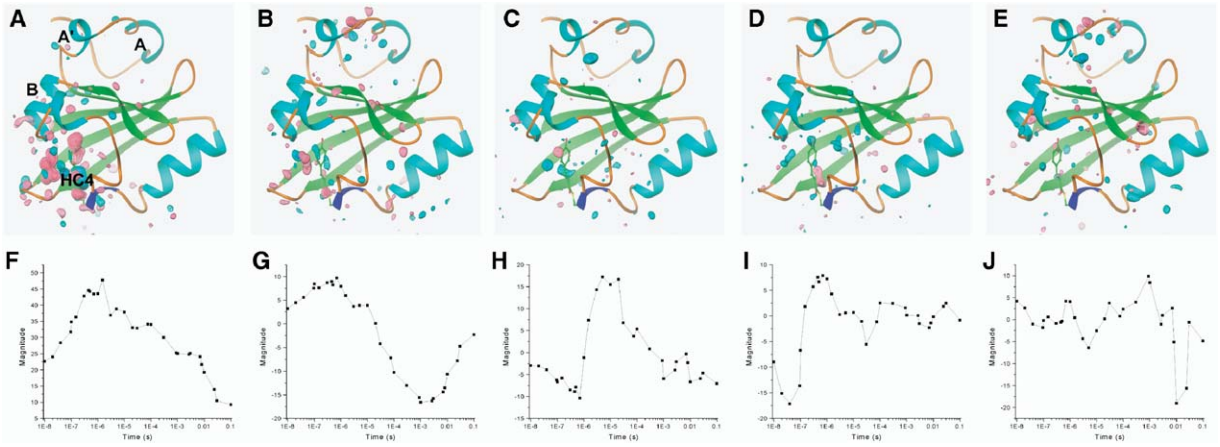

Figure 1. Views of Left Singular Vectors and Right Singular Vectors 1–4 and 6

(A–E) Difference electron density of left singular vectors (lSVs) 1–4 and 6, respectively, contoured at −6σ (red), −3.5σ (pink), +3.5σ (cyan), and +6σ (blue). In a difference map, negative difference electron density, which is found in those regions from which atoms have moved relative to their position in the dark state, is shown in pink and red, and positive difference electron density, which is found in those regions to which atoms have moved in their new state, is shown in cyan and blue. In the lSVs, the sign of these features is arbitrary since they are linear combinations of the underlying intermediate difference electron density. Therefore, in regions that undergo conformational changes, one would expect to observe flanking negative and positive difference features, corresponding to shifts in atomic coordinates.

(F–J) Magnitudes of right singular vectors (rSVs) 1–4 and 6, respectively, weighted by the square of their corresponding singular value plotted against time.

in reciprocal space, Anderson et al. (2004b) identified and refined the structures of the early red-shifted intermediate pR (or I_1) and the late blue-shifted intermediate pB (or I_2). However, this method of analysis assumes that the structure is homogeneous throughout the two selected time ranges and precludes a detailed study of the time domain of the photocycle. Their quantitative analysis was also restricted to the chromophore and its binding pocket. Only qualitative information was available on the surrounding protein, since their method of analysis tended to average out structural changes. A more quantitative analysis of this data would allow for a determination of E46Q PYP's chemical kinetic mechanism and a comparison of it to the mechanism of WT PYP (Schmidt et al., 2004; Ihee et al., submitted).

We apply SVD analysis to the 30 E46Q PYP data sets from 10 ns to 100 ms of Anderson et al. (2004b). This analysis yields a complete description of the E46Q PYP photocycle in the crystal and identifies a structural mechanism by which a signal generated at the chromophore binding pocket is transduced to other regions of the protein.

Results

SVD Analysis of Data

From our SVD analysis of the data at 30 time points, we identified only 5 of the total 30 left singular vectors (lSVs) as being significant, namely, lSVs 1–4 and 6 (Rajagopal et al., 2004a). These lSVs, each of which is a linear combination of the difference electron density associated with each intermediate (see below), show significant features in the chromophore binding pocket, helix B, and helix A′ and smaller but still significant features in the surrounding protein (Figures 1A–1E). Residual maps generated from the remaining lSVs, 5 and 7–30, do not show persistent difference electron density from time point to time point (Rajagopal et al., 2004a), which confirms that the five selected lSVs are sufficient to describe the signal present in the data. The right singular vectors (rSVs) describe the time dependence of the corresponding lSVs and are a linear combination of the concentrations of the intermediates, weighted by the square of the singular values; these are shown in Figures 1F–1J. These rSVs are well behaved and can be globally fit with four relaxation times (233 ns, 1.54 μs, 84 μs, and 14 ms) (Rajagopal et al., 2004a).

Based on the number of relaxation times (four) and the number of significant singular vectors (five) (Henry and Hofrichter, 1992; Schmidt et al., 2003), we fit the rSVs by using candidate chemical kinetic mechanisms containing six structural states, namely, a ground state and five intermediate states, which we refer to as IE1, IE2, IL1, IL2, and IL3 (for intermediate, early, and late). At this stage, a fit to the rSVs will yield nearly identical difference density maps for intermediates in each candidate mechanism that is similar to the correct chemical kinetic mechanism (Schmidt et al., 2003). The general model we use as a basis for evaluating candidate mechanisms is shown in Figure 2A. Fitting with an irreversible sequential mechanism that includes a side path directly from IE1 to IL1 (Figure 2B) resulted in a good fit to the rSVs (Figure 2C), with the exception of three early time points of rSV 4 and three late time points of rSV 6. This tentative fit allowed the time-independent difference electron density associated with each intermediate to be calculated and, after refinement of structural models for all intermediates, the final chemical kinetic mechanism to be determined. Other analytic methods, such as target analysis (van Stokkum et al., 2004), may become important tools for the determination of chemical kinetic mechanism with data of higher signal-to-noise than the present, which has significant systematic errors (Rajagopal et al., 2004a, 2004b).

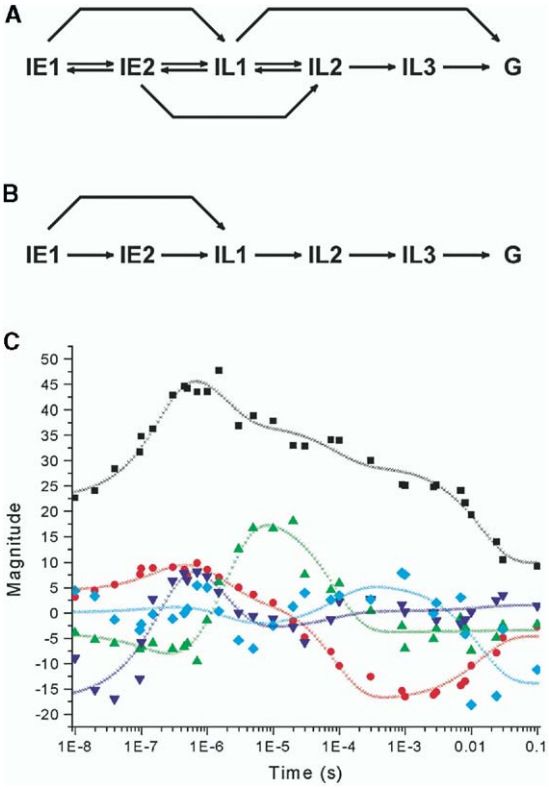

Figure 2. Candidate Mechanisms and Fits of the rSVs

(A) General model for a candidate mechanism.

(B) Branched model used to fit the rSVs.

(C) Fit of rSVs 1–4 and 6 (black, red, green, blue, and cyan, respectively) to the branched model with rate coefficients (s^{-1}) of 3.8 × 10^6 (IE1 → IE2), 1.3 × 10^6 (IE1 → IL1), 7.0 × 10^5 (IE2 → IL1), 1.1 × 10^4 (IL1 → IL2), 25 (IL2 → IL3), and 0 (IL3 → G).

Structural Progression in the Photocycle

The difference electron densities for the five intermediates are shown in Figure 3. The difference electron density maps of the two early states, IE1 and IE2 (Figures 3A, 3B, 3F, and 3G), are very similar to each other. Most features are limited to the chromophore binding pocket. Strong negative features on the dark state chromophore structure, most notably the phenolate oxygen and the carbonyl oxygen, are consistent with isomerization of the chromophore, and positive difference features near the chromophore are consistent with those characteristic of the pR spectroscopic state (Anderson et al., 2004b). Negative and associated positive features on Arg52 suggest that this side chain is pushed to the edge of the pocket by the isomerized chromophore. IE2 has slightly more features distant from the chromophore binding pocket than IE1 (Figures 3A and 3B), suggesting that structural changes have started to propagate out from the chromophore in IE2.

The two late intermediates, IL1 and IL2, have features in the chromophore binding pocket (Figures 3H and 3I) similar to those associated with pB difference density (Anderson et al., 2004b; Genick et al., 1997a). One major feature is the extended positive density behind the dark state chromophore that is associated with the *cis* chromophore of pB. In contrast to IE1 and IE2, IL1 and IL2 display a number of strong features outside the chromophore binding pocket (Figures 3C and 3D). These clearly indicate tertiary structural changes distant from the chromophore; for example, positive and negative features lie along the length of helix B flanking the dark state density. The major difference between IL1 and IL2 lies in the N terminus on helix A′, where IL2 has strong features that IL1 lacks (Figure 3D). In the last intermediate, IL3, the chromophore binding pocket is almost completely devoid of features (Figure 3J), which demonstrates that the chromophore has returned to its *trans*, dark state conformation. Nevertheless, strong features persist on helix A′ (Figure 3E).

By inspection of the difference features of all five intermediates (Figures 3A–3E), a clear structural progression is evident from the early to the late intermediates. In IE1 and IE2, the signal is restricted to the chromophore binding pocket, from which it progresses

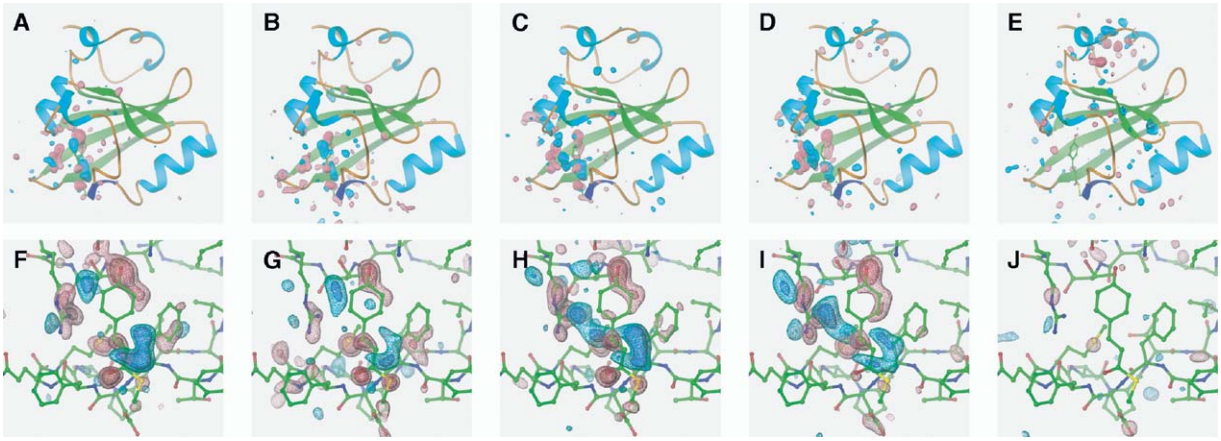

Figure 3. Difference Electron Densities Associated with the Intermediates

(A–J) (A–E) Entire protein and (F–J) chromophore binding pocket views of difference electron densities associated with intermediates IE1, IE2, IL1, IL2, and IL3, respectively. The dark state E46Q PYP model is shown for clarity. Difference maps are contoured at –4σ (red), –3σ (pink), +3σ (cyan), and +4σ (blue).

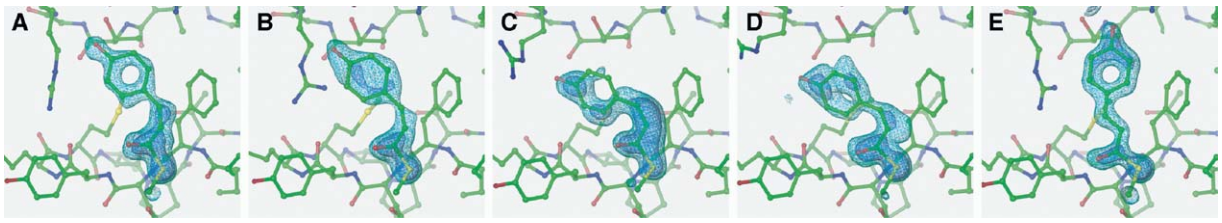

Figure 4. Structures and Extrapolated Electron Densities

(A–E) Refined structures and associated extrapolated electron densities that simulate complete photoactivation of intermediates IE1, IL2, IL1, IL2, and IL3, respectively. Maps are contoured at +1σ (cyan) and +2σ (blue).

to helix B in IL1, and finally to helix A′ of the N terminus in IL2. In the last intermediate, IL3, the chromophore has relaxed back to its dark state conformation, while strong difference features persist at the N terminus.

Intermediate Structures

From the Fourier back-transformed difference electron density, we performed difference refinement (Terwilliger and Berendzen, 1995) of each intermediate. Refined structures of the chromophores for each intermediate are superimposed on their extrapolated density in Figure 4. Real space correlation coefficients (Vaguine et al., 1999) were above 0.8 for all residues in each intermediate model, with the exception of two residues in the βV-βVI loop in IL2 and Arg52 in the IL1 and IL2 structures. The former is a region of high temperature factors in the dark state structure, and the latter probably arises from disorder in Arg52 after its ejection from the chromophore binding pocket. The two early intermediates, IE1 (Figure 4A) and IE2 (Figure 4B), have similar chromophore structures to that of pR (Anderson et al., 2004b): the hydrogen bond between the chromophore phenolate oxygen and Gln46 is completely broken, but the unusually short hydrogen bond (Anderson et al., 2004a) between the phenolate oxygen and Tyr42 present in the dark state (2.49 Å) is slightly lengthened but preserved (2.7 Å) (Table 1). The major difference between the IE1 and IE2 intermediates lies in the position of the phenolate oxygen, with the consequence that its hydrogen bond to Tyr42 is further lengthened to 3.2 Å in IE2, still below our distance cutoff of 3.3 Å (CCP4, 1994) (Table 1). In both IE1 and IE2, Arg52 is only displaced slightly out of the pocket by the isomerized chromophore; its hydrogen bonds to the backbone carbonyls of Tyr98 and Thr50 are lengthened but preserved.

The two late intermediates, IL1 (Figure 4C) and IL2 (Figure 4D), have chromophore conformations similar to the refined pB conformation (Anderson et al., 2004b): the chromophore hydrogen bonding network is completely disrupted, and the chromophore has swung down (to the left: Figure 4) and completely ejected the side chain of Arg52 from the binding pocket. In IL2, the conformation of the tail of the chromophore, comprised of its carbonyl group and cysteine sulfur, differs from that in IL1 in that the hydrogen bond between the chromophore carbonyl oxygen and the backbone amide hydrogen of Cys69 is shortened from 3.2 Å in IL1 to 2.9 Å in IL2 (Table 1). These two chromophore conformations correspond well to the two late intermediate structures of WT PYP refined by Schmidt et al. (2004). Both IL1 and IL2 have small backbone shifts (~0.2 Å) along helix B, and IL2 has larger backbone shifts (~0.4 Å) along helix A′, consisting of residues 11–20, relative to the dark state conformation. In IL3 (Figure 4E), reisomerization about the C2-C3 bond results in the adoption of a chromophore binding pocket conformation nearly identical to that of the dark state, but the backbone shifts in helix A′ present in IL2 are maintained.

The Chemical Kinetic Mechanism of E46Q PYP

In fitting a candidate chemical kinetic mechanism to maps reconstituted with the five rSVs, 1–4 and 6, only a quarter of all data was fit (Rajagopal et al., 2004a), and the scale of the intermediate difference density was not taken into account (Schmidt et al., 2003). The intermediate structures must be globally fit to all 30 SVs in order to determine a chemical kinetic mechanism based on the general model shown in Figure 2A. Fitting with an irreversible sequential mechanism including a side path from IL1 directly to the dark state (shown in Figure 5A) resulted in a lower total square deviation

Table 1. Geometry of the Chromophore Environment

	O4′-Tyr42	O4′-Gln46	O1-Cys69	Tyr42-Thr50	DP
IE1	2.7	5.5	3.3	2.8	0.23
IE2	3.2	5.9	2.9	2.8	0.23
IL1	5.5	7.9	3.2	2.6	0.42
IL2	5.4	7.7	2.9	2.8	0.45
IL3	2.4	3.0	2.8	2.9	0.22
Dark	2.49	2.87	2.80	2.84	0.21

Relevant atom-to-atom distances (in Å) and deviation from planarity of the chromophore (by using atoms from the cysteine sulfur of Cys69 to the chromophore phenolate oxygen) of the five structural intermediates during the E46Q PYP photocycle. O1, the chromophore carbonyl oxygen; O4′, the chromophore phenol(ate) oxygen; Tyr42, the hydroxyl oxygen of Tyr42; Gln46, the Nε2 of Gln46; Cys69, the backbone amide nitrogen of Cys69; Thr50, the Oγ of Thr50; DP, rmsd from planarity of the chromophore from the sulfur of Cys69 to the phenolate oxygen. DPs were calculated by using the CCP4 program GEOMCALC (CCP4, 1994). The structure used for the dark state is from Anderson et al. (2004a).

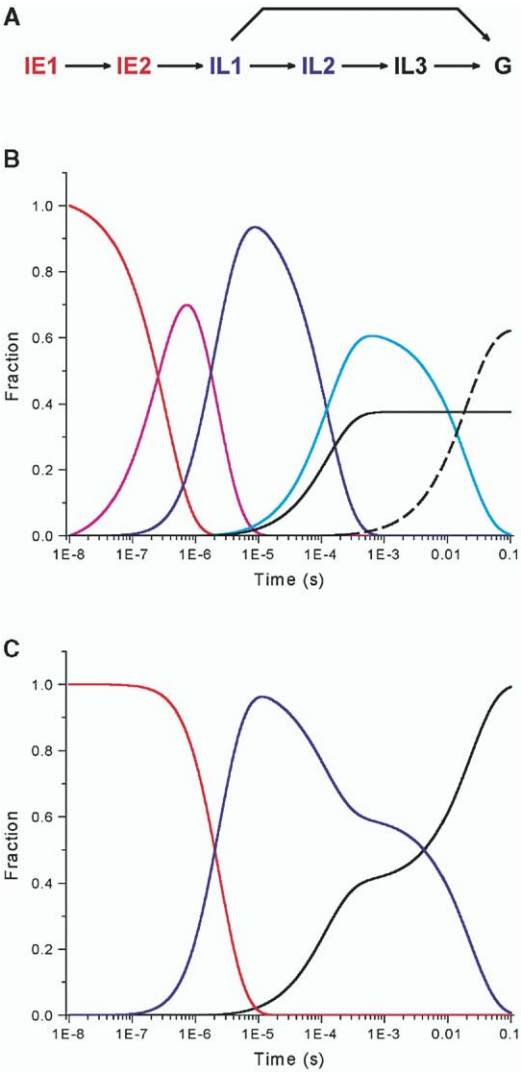

Figure 5. The Chemical Kinetic Mechanism of E46Q PYP in the Crystal

(A) Chemical kinetic mechanism of E46Q PYP in the crystal, with rate coefficients (s^{-1}) of 3.0×10^6 (IE1→IE2), 5.0×10^5 (IE2→IL1), 5.0×10^3 (IL1→IL2), 3.0×10^3 (IL1→G), 50 (IL2→IL3), and 0 (IL3→G).

(B) Predicted concentrations of IE1 (red), IE2 (magenta), IL1 (blue), IL2 (cyan), IL3 (dashed), and the ground state (black) with the mechanism in (A).

(C) Predicted concentration profiles for spectroscopic intermediates pR (IE1 and IE2) shown in red, pB (IL1 and IL2) shown in blue, and the ground state (IL3 and pG) shown in black with the mechanism in (A).

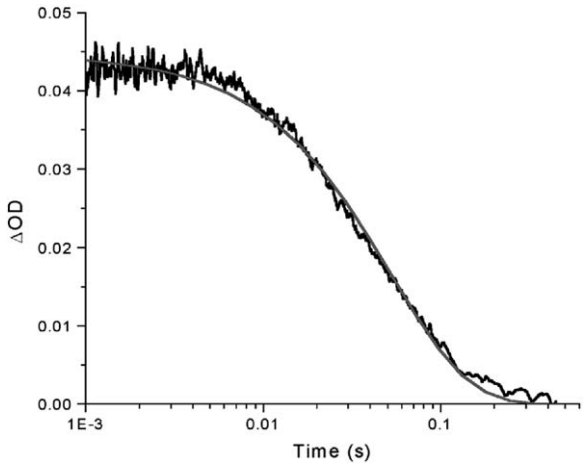

Figure 6. Photosensitivity of Crystals

Recovery of ground state absorption in a crystalline state monitored at 488 nm after excitation by a pulse at 500 nm. Shown in gray is a fit to a single exponential with a relaxation time of 15 ms.

than other models of similar complexity. The inclusion of additional rate coefficients did not significantly change the total square deviation. This mechanism is broadly consistent with the photocycle of crystalline WT PYP, in which the relaxation of the two late intermediates to the dark state is not sequential (Schmidt et al., 2004). The concentrations for individual intermediates predicted by this mechanism are shown in Figure 5B. It is evident from this that, first, at nearly all times multiple structural intermediates are populated and, second, the pR and pB spectroscopic states are structurally heterogeneous, i.e., a single state identified by visible absorption spectroscopy corresponds to multiple structural states. Also, data collection did not span a sufficiently long time range to fully capture the final relaxation of IL3 back to the ground state. We emphasize that this mechanism (Figure 5A) contains the minimum number of states and rate coefficients necessary to account for our data. Our analysis, however, does not exclude other steps in the mechanism whose addition may modestly improve the total square deviation within the high noise level of the data.

Based on chromophore conformation (Figure 4), IE1 and IE2 can be assigned to a pR-like absorption spectrum, IL1 and IL2 to a pB-like absorption spectrum, and IL3 to a dark state-like absorption spectrum. From our candidate mechanism, we predict the concentrations of the pR, pB, and dark spectroscopic states in the crystal (Figure 5C) and compare them to the kinetics of dark state recovery of a crystalline slurry of E46Q PYP measured optically (Figure 6). Since the time resolution of the microspectrophometry is limited to milliseconds, we cannot identify the faster phase of the recovery in which IL1 is predicted to decay directly to the dark state. However, the kinetic trace is well fit with a single relaxation of τ = 15 ms (Figure 6), very close to the relaxation time of 20 ms for the IL2 to IL3 transition in our crystallographic analysis (dashed line in Figure 5B).

Discussion

Structural and Spectroscopic Intermediates

Two major species have been identified by visible absorption spectroscopy during the PYP photocycle: pR and pB (Hellingwerf et al., 1996; Meyer et al., 1987). Our results show that the pR and pB visible absorption states each correspond to at least two structurally distinct intermediates, consistent with other spectroscopic findings (Brudler et al., 2001; Rubinstenn et al., 1998). In the pR-like intermediates IE1 and IE2, predicted to have a red-shifted absorption, the chromophore has isomerized to *cis*, and only the hydrogen

bond between Tyr42 and the chromophore phenolate oxygen is preserved, but lengthened relative to the dark state. The chromophore conformation is closely similar to the single pR species refined by Anderson et al. (2004b). In all of these structures, the hydrogen bond between the phenolate oxygen and Gln46 is broken, in contrast to low-temperature (Anderson et al., 2004a; Genick et al., 1998) and FT-IR experiments (Brudler et al., 2001; Imamoto et al., 2001) that have noted that this hydrogen bonding network is preserved in early intermediates. New time-resolved Laue experiments (Ihee et al., submitted) on WT PYP suggest that the structures present at low temperature (Anderson et al., 2004a; Genick et al., 1998) correspond to early intermediates that are populated in the room temperature photocycle from hundreds of picoseconds to a few nanoseconds; while FT-IR experiments probe a heterogeneous state consisting of two species, only one of which preserves the hydrogen bond (Unno et al., 2004). Thus, it is likely that E46Q PYP structures observed at low temperature that preserve the hydrogen bond (Anderson et al., 2004a) precede the IE1 intermediate at room temperature.

In the pB-like intermediates IL1 and IL2, predicted to have a blue-shifted absorption, the chromophore has largely relaxed in the *cis* conformation and is protonated (Genick et al., 1997a). The major difference in chromophore conformation between IL1 and IL2 lies in the position of the chromophore carbonyl oxygen relative to the backbone amide hydrogen of residue 69. The hydrogen bond between these groups is substantially shorter in IL2 than in IL1, resulting in a conformation of the chromophore tail that is more similar to that of the dark state. We interpret this strengthening of the proximal hydrogen bonding network of the chromophore to the surrounding protein as a lowering of the energetic barrier for subsequent thermal *cis-trans* reisomerization of the chromophore. We do not identify any other intermediates on the pathway of this reisomerization, which also requires adjustment of the pKa of the chromophore, its reinsertion into its pocket, and reestablishment of the hydrogen bonding network. For a reisomerization intermediate to be directly observed in any ensemble measurement, it would have to build up quickly and decay slowly, which is unlikely in such an energetically downhill process.

We do identify a novel intermediate after chromophore reisomerization, IL3, whose chromophore conformation shows no differences from the dark state, but which retains the strong structural shifts in residues 11–20 of its N terminus that are found in the earlier intermediate, IL2. This reisomerized intermediate may be analogous to substates in the N and O intermediates of bR, where the processes of proton uptake, reprotonation, and chromophore isomerization are not necessarily simultaneous (reviewed in Balashov and Ebrey, 2001). The visible absorption spectrum of the IL3 intermediate is predicted to be indistinguishable from that of the dark state. Its presence accounts for the different rates for protein and chromophore relaxation to the dark state in the earlier analysis of the time-resolved data by Anderson et al. (2004b). It is unlikely that the presence of this intermediate is a crystal packing artifact: the region of the N terminus that undergoes the most significant structural changes (residues 11–20) is packed against the βII and βIII regions of an adjacent molecule, two regions which are largely devoid of structural signal during the photocycle. The N-capping motif that we propose transduces the structural signal from the chromophore to the N terminus is fully solvent exposed (see below), and the structural signal is consistent with previous experiments performed in solution (see below).

A Structural Pathway for Energy Transduction

Our time-resolved data directly visualize a temporal and spatial pathway for progression of structural change from the chromophore and its binding pocket, through helix B, to the N terminus. The N terminus of the protein has previously been identified as a region that undergoes significant structural changes in a photostationary state of WT PYP (Rubinstenn et al., 1998). Light-dependent unfolding of the two N-terminal helices (Craven et al., 2000; Imamoto et al., 2002), A and A′, is responsible for the heat capacity changes associated with the PYP photocycle (van der Horst et al., 2001), and N-terminal deletion mutants have a 10- to 100-fold decrease in the rate of recovery of the dark state (Harigai et al., 2001; van der Horst et al., 2001). In previous time-resolved Laue experiments, more significant N-terminal structural changes were observed in E46Q PYP than in WT PYP (Schmidt et al., 2004), while, in solution, the converse is true, with N-terminal structural changes in E46Q PYP of a more limited nature than in WT PYP (Derix et al., 2003). In a more recent WT PYP Laue experiment (Ihee et al., submitted), N-terminal structural changes similar to those in E46Q PYP have been observed. In all of these crystallographic experiments, the features observed in the original difference maps (Anderson et al., 2004b) associated with limited structural shifts near the N terminus may represent precursors to more extensive N-terminal unfolding in solution that are present in both WT and E46Q PYP. Subsequent unfolding in E46Q PYP is likely limited due to its faster reisomerization to the dark state relative to WT PYP. Unfolding competes with reisomerization.

How is the structural signal, originating in the prompt isomerization of the chromophore, transduced to the N terminus of the protein? In the dark state, helix B is tethered to the chromophore phenolate oxygen by a hydrogen bonding network involving residues Gln46, Thr50, and Tyr42, the last of which forms an unusually short (2.49 Å) and putatively stable hydrogen bond (Anderson et al., 2004a). Arg52, positioned at the C-terminal end of helix B, acts as a gate between the chromophore and solvent in the dark state and is further stabilized by hydrogen bonds between its guanidine group and the backbone carbonyl oxygens of Tyr98 and Thr50. After absorption of a photon, structural changes in the early intermediates are limited to the chromophore binding pocket. In IE1 and IE2, only the hydrogen bond between Gln46 and the chromophore phenolate oxygen is broken; that between Tyr42 and the phenolate oxygen remains short in IE1 (2.6 Å), but extends to 3.2 Å in IE2. In IL1, the chromophore adopts a fully relaxed *cis* conformation. This breaks the last remaining hydrogen bond between the chromophore and Tyr42, and the chromophore ejects Arg52 into the solvent, breaking its hydrogen bonds to Tyr98 and Thr50. In this

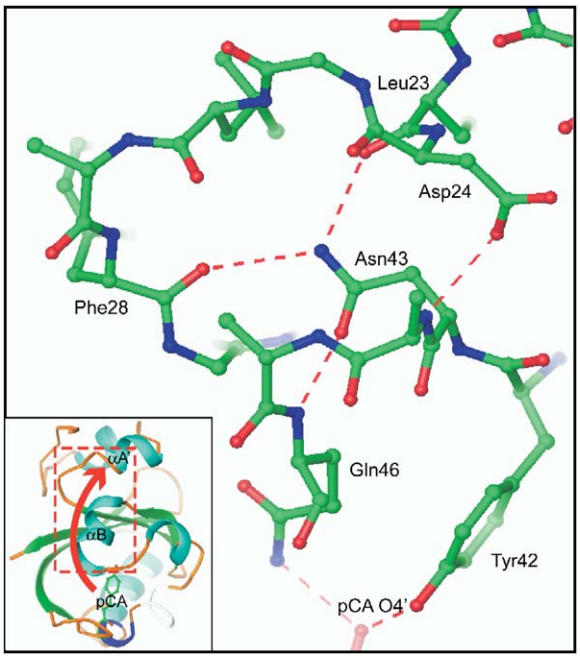

Figure 7. A Conserved Helix Capping Motif in PYP that Links Helices B and A′

The side chain of Asn43 is hydrogen bonded (dashed lines) to three atoms: through its carbonyl moiety, it hydrogen bonds to the backbone amide of Gln46, and through its amine moiety, it hydrogen bonds to the backbone carbonyl oxygens of Phe28 and Leu23. In WT PYP, two of these hydrogen bonds, to Glu46 and Phe28, are broken or significantly weakened in the pB state (Craven et al., 2000). Shown also are the hydrogen bonds between the chromophore phenolate oxygen (pCA O4′) and the side chains of Gln46 and Tyr42. Removed for clarity are residues 47–51.

step, all hydrogen bonds that initially tethered helix B to the chromophore are broken. This allows helix B to shift up toward the N terminus by ~0.2 Å; this signal, in IL2, is propagated to the N terminus through a helix-capping interaction involving Asn43 and Asp24 (Figure 7).

Asn43 is a very highly conserved residue in both PYPs and in PAS domains more generally (Taylor and Zhulin, 1999). In PYPs, the side chain of Asn43 forms two key hydrogen bonds. By the hydrogen bond between its carbonyl moiety and the backbone amide of Gln46, Asn43 stabilizes helix B by the common N-capping motif (Richardson and Richardson, 1988). Hydrogen bonds between its amine moiety and the backbone carbonyl oxygens of Leu23 and Phe28 further link helix B to helix A′ (Figure 7). Similarly, the side chain of Asp24 in helix A′ is hydrogen bonded to the backbone nitrogen of Ala44 of helix B. Thus, Asn43 and Asp24 provide a hydrogen bonding network that bridges these two helices (Figure 7) and can couple structural changes between them. In WT PYP, the hydrogen bonds between Asn43 and Glu46 and between Asn43 and Phe28 are two of the three most significantly deprotected in the photostationary state relative to the dark state, as assessed by H/D exchange (Craven et al., 2000). In solution, disruption of this highly conserved interaction may then lead to destabilization and then unfolding of the N-terminal helices; in the crystal, N-terminal unfolding is prevented by crystalline lattice forces. In IL3, the chromophore relaxes back to its dark state conformation and reestablishes its hydrogen bonding network to helix B, while structural changes persist at the N terminus. Thus, the relaxations of the chromophore and the protein to the dark state are not coupled strongly, which is surprising for such a small protein.

The structural pathway from the chromophore binding pocket through helix B and terminating at helix A′ allows structural signals generated at the chromophore to be transmitted to the N terminus, a distance of over 20 Å. Recently, light-dependent unfolding of a helix, such as that observed in PYP (Harigai et al., 2001; van der Horst et al., 2001), has been observed in the LOV domain (Harper et al., 2003), a flavin binding PAS domain, suggesting a more general mechanism of helix order/disorder for signaling (Cusanovich and Meyer, 2003) in the photosensory PAS domains. In the LOV domains, it is a C-terminal helix that unfolds. The residue analogous to Asn43 is a serine, which is capable of acting as an N-cap but not of propagating the signal farther. This suggests that although the general structural signal, i.e., helix order/disorder, may be conserved across PAS domains, there are likely to be rather different mechanisms for its generation.

Conclusions

The application of singular value decomposition to this set of time-resolved crystallographic data spanning the photocycle of the E46Q mutant of PYP from 10 ns to 100 ms has allowed us to identify five distinct structural intermediates and provide a plausible chemical kinetic mechanism for the photocycle. This sequence of intermediates shows a distinct progression of structural changes that follows a clear pathway through the protein, originating at the chromophore, proceeding through helix B, and ending at the N terminus. This pathway contains a number of highly conserved residues in PYPs and PAS domains and suggests that this mechanism for generating the structural signal may apply to PAS domains in general.

Experimental Procedures

Data Preparation and Evaluation

Anderson et al. (2004b) and Anderson (2003) provide details on experimental data collection and extraction of structure factor amplitudes. A total of 54 Laue data sets corresponding to 30 different time points spanning the photocycle of the E46Q mutant of PYP from 10 ns to 100 ms were collected at beamline 14-ID-B of the Advanced Photon Source and beamline ID09 of the European Synchrotron Radiation Facility. Rajagopal et al. (2004a) discuss the application of SVD to this data. SVD decomposes time-dependent data from a data matrix, $\boldsymbol{A}$, into three matrices (Henry and Hofrichter, 1992): $\boldsymbol{A} = \boldsymbol{USV}^T$, where $\boldsymbol{V}^T$ denotes the transpose of matrix $\boldsymbol{V}$. In the analysis of time-dependent difference electron density, $\boldsymbol{U}$ is composed of left singular vectors (lSVs), a basis set for time-independent difference electron density; $\boldsymbol{S}$ is composed of the singular values, weighting factors for their corresponding singular vectors; and $\boldsymbol{V}$ is composed of the right singular vectors (rSVs), which describe the time dependence of the corresponding lSVs. Selection of significant SVs allows reconstitution of the data matrix $\boldsymbol{U}'\boldsymbol{S}'\boldsymbol{V}'^T = \boldsymbol{A}' \sim \boldsymbol{A}$. The significant rSVs were then globally fit with a ′ sum of exponentials. In later stages, they were fit with different candidate mechanisms according to $\boldsymbol{V}' = \boldsymbol{CP}$, where $\boldsymbol{C}$ is a set of intermediate concentrations based on a candidate mechanism, and $\boldsymbol{P}$ is a set of linear parameters (Henry and Hofrichter, 1992). The time-independent difference electron densities of the intermediates for this candidate mechanism, denoted by the matrix $\boldsymbol{F}$, were

then extracted as follows: since $FC^T = A' = U' S' V'^T = U' S' P^T C^T$, then $F = U' S' P^T$.

Difference Refinement

Difference structure factors and phases were calculated from the intermediate difference density maps by Fourier backtransformation. Difference refinement (Terwilliger and Berendzen, 1995) against this data extending to 1.6 Å was performed in SHELX-97 (Sheldrick and Schneider, 1997), and model building and viewing of electron density maps was performed in XtalView (McRee, 1999). The model used for refinement was a mixture of dark state PYP, whose parameters, except for fractional occupancy, were not varied, and an intermediate state, all of whose parameters were varied. The sum of the fractional occupancies of the dark and each intermediate state was fixed at unity, and multiple cycles of restrained conjugate gradient least squares refinement were performed. While we monitored the relative values of R factor and R_{free} during refinement, we do not consider them suitable absolute measures of the quality of the model because they vary with the occupancy of the intermediate (Anderson, 2003). Therefore, we carefully evaluated $F_o - F_c$ residual maps and the fit of the chromophore to extrapolated electron density maps simulating 100% photoinitiation that were generated by multiplying ΔF by an occupancy factor and adding it to F_c^{dark}. After refinement, real space correlation coefficients were calculated in SFCHECK (Vaguine et al., 1999) to ensure the quality of the refined models.

Posterior Analysis

Difference electron density calculated from the structures of the refined intermediates was used in posterior analysis, a process in which the original SVD-flattened maps are fit with intermediate difference electron density by using different candidate mechanisms (discussed in Schmidt et al., 2003). A number of candidate models based on the general scheme shown in Figure 2A were used to fit the data. Models were assessed by the magnitude of the total squared deviation over all 30 time delays of features above the $+3\sigma$ or below the -3σ level in the observed or calculated maps. The mechanism that resulted in the lowest total square deviation within the experimental noise and involved the fewest reaction steps was chosen as the minimal model; the chosen model is consistent with the crystallographic data.

Crystal Microspectrophotometry

Microspectrophotometry of slurries of E46Q PYP crystals was performed at 14°C as described (Chen et al., 1994). Absorption spectra were collected with a diode array spectrometer (USB2000 Fiber Optic Spectrometer from Ocean Optics). Millisecond kinetics were collected by using a nanosecond solid-state laser (Vibrant Tunable Laser System, Model VIS II/UV from Opotek) tuned to 500 nm as a pump pulse and an argon ion laser (5425ASL-00 Ar Ion laser from Ion Laser Technology) tuned to 488 nm as a probe. The signal was detected by using a photomultiplier tube (Hamamatsu R955 PMT) monitored with an oscilloscope (500 MHz Tektronix 744A). Kinetic traces could not be analyzed at times shorter than 500 μs due to recovery of the photomultiplier tube from the excitation flash. Traces were fit in Origin 6.1 (Microcal, Inc.).

Acknowledgments

We thank Hyotcherl Ihee, Jason Key, Sean Crosson, and Wouter Hoff for valuable discussions. This work was supported by National Institutes of Health grants GM36452 and RR07707 to K.M. M.S. was supported by Sonderforschungsbereich 533 of the Deutsche Forschungsgemeinschaft.

Received: July 22, 2004
Revised: October 21, 2004
Accepted: October 21, 2004
Published: January 11, 2005

References

Anderson, S. (2003). Formation of a new buried charge drives a large-amplitude protein quake in photoreceptor activation.

Anderson, S., Srajer, V., Crosson, S., and Moffat, K. (2004a). Short hydrogen bonds in photoactive yellow protein. Acta Crystallogr. D Biol. Crystallogr. *60*, 1008–1016.

Anderson, S., Srajer, V., Pahl, R., Rajagopal, S., Schotte, F., Anfinrud, P., Wulff, M., and Moffat, K. (2004b). Chromophore conformation and the evolution of tertiary structural changes in photoactive yellow protein. Structure *12*, 1039–1045.

Balashov, S.P., and Ebrey, T.G. (2001). Trapping and spectroscopic identification of the photointermediates of bacteriorhodopsin at low temperatures. Photochem. Photobiol. *73*, 453–462.

Brudler, R., Rammelsberg, R., Woo, T.T., Getzoff, E.D., and Gerwert, K. (2001). Structure of the I1 early intermediate of photoactive yellow protein by FTIR spectroscopy. Nat. Struct. Biol. *8*, 265–270.

CCP4 (Collaborative Computational Project, Number 4)(1994). The CCP4 suite: programs for protein crystallography. Acta Crystallogr. D Biol. Crystallogr. *50*, 760–763.

Chen, Y., Srajer, V., Ng, K., Legrand, A., and Moffat, K. (1994). Optical monitoring of protein crystals in time-resolved x-ray experiments—microspectrophotometer design and performance. Rev. Sci. Instrum. *65*, 1506–1511.

Craven, C.J., Derix, N.M., Hendriks, J., Boelens, R., Hellingwerf, K.J., and Kaptein, R. (2000). Probing the nature of the blue-shifted intermediate of photoactive yellow protein in solution by NMR: hydrogen-deuterium exchange data and pH studies. Biochemistry *39*, 14392–14399.

Crosson, S., Rajagopal, S., and Moffat, K. (2003). The LOV domain family: photoresponsive signaling modules coupled to diverse output domains. Biochemistry *42*, 2–10.

Cusanovich, M.A., and Meyer, T.E. (2003). Photoactive yellow protein: a prototypic PAS domain sensory protein and development of a common signaling mechanism. Biochemistry *42*, 4759–4770.

Derix, N.M., Wechselberger, R.W., van der Horst, M.A., Hellingwerf, K.J., Boelens, R., Kaptein, R., and van Nuland, N.A. (2003). Lack of negative charge in the E46Q mutant of photoactive yellow protein prevents partial unfolding of the blue-shifted intermediate. Biochemistry *42*, 14501–14506.

Frauenfelder, H., McMahon, B.H., Austin, R.H., Chu, K., and Groves, J.T. (2001). The role of structure, energy landscape, dynamics, and allostery in the enzymatic function of myoglobin. Proc. Natl. Acad. Sci. USA *98*, 2370–2374.

Genick, U.K., Borgstahl, G.E., Ng, K., Ren, Z., Pradervand, C., Burke, P.M., Srajer, V., Teng, T.Y., Schildkamp, W., McRee, D.E., et al. (1997a). Structure of a protein photocycle intermediate by millisecond time-resolved crystallography. Science *275*, 1471–1475.

Genick, U.K., Devanathan, S., Meyer, T.E., Canestrelli, I.L., Williams, E., Cusanovich, M.A., Tollin, G., and Getzoff, E.D. (1997b). Active site mutants implicate key residues for control of color and light cycle kinetics of photoactive yellow protein. Biochemistry *36*, 8–14.

Genick, U.K., Soltis, S.M., Kuhn, P., Canestrelli, I.L., and Getzoff, E.D. (1998). Structure at 0.85 Å resolution of an early protein photocycle intermediate. Nature *392*, 206–209.

Harigai, M., Yasuda, S., Imamoto, Y., Yoshihara, K., Tokunaga, F., and Kataoka, M. (2001). Amino acids in the N-terminal region regulate the photocycle of photoactive yellow protein. J. Biochem. (Tokyo) *130*, 51–56.

Harper, S.M., Neil, L.C., and Gardner, K.H. (2003). Structural basis of a phototropin light switch. Science *301*, 1541–1544.

Hellingwerf, K.J. (2002). The molecular basis of sensing and responding to light in microorganisms. Antonie Van Leeuwenhoek *81*, 51–59.

Hellingwerf, K.J., Hoff, W.D., and Crielaard, W. (1996). Photobiology of microorganisms: how photosensors catch a photon to initialize signalling. Mol. Microbiol. *21*, 683–693.

Hellingwerf, K.J., Hendriks, J., and Gensch, T. (2003). Photoactive yellow protein, a new type of photoreceptor protein: will this "yellow lab" bring us where we want to go? J. Phys. Chem. A *107*, 1082–1094.

Henry, E., and Hofrichter, J. (1992). Singular value decomposition: application to analysis of experimental data. Methods Enzymol. *210*, 129–192.

Hoff, W.D., Xie, A., van Stokkum, I.H., Tang, X.J., Gural, J., Kroon, A.R., and Hellingwerf, K.J. (1999). Global conformational changes upon receptor stimulation in photoactive yellow protein. Biochemistry *38*, 1009–1017.

Imamoto, Y., Shirahige, Y., Tokunaga, F., Kinoshita, T., Yoshihara, K., and Kataoka, M. (2001). Low-temperature Fourier transform infrared spectroscopy of photoactive yellow protein. Biochemistry *40*, 8997–9004.

Imamoto, Y., Kamikubo, H., Harigai, M., Shimizu, N., and Kataoka, M. (2002). Light-induced global conformational change of photoactive yellow protein in solution. Biochemistry *41*, 13595–13601.

Lim, W.A. (2002). The modular logic of signaling proteins: building allosteric switches from simple binding domains. Curr. Opin. Struct. Biol. *12*, 61–68.

McRee, D.E. (1999). XtalView/Xfit: a versatile program for manipulating atomic coordinates and electron density. J. Struct. Biol. *125*, 156–165.

Meyer, T.E., Yakali, E., Cusanovich, M.A., and Tollin, G. (1987). Properties of a water-soluble, yellow protein isolated from a halophilic phototrophic bacterium that has photochemical activity analogous to sensory rhodopsin. Biochemistry *26*, 418–423.

Rajagopal, S., Schmidt, M., Anderson, S., and Moffat, K. (2004a). Analysis of experimental time-resolved crystallographic data by singular value decomposition. Acta Crystallogr. D Biol. Crystallogr. *60*, 860–871.

Rajagopal, S., Kostov, K., and Moffat, K. (2004b). Analytical trapping: extraction of time-independent structures from time-dependent crystallographic data. J. Struct. Biol. *147*, 211–222.

Ren, Z., Bourgeois, D., Helliwell, J., Moffat, K., Srajer, V., and Stoddard, B. (1999). Laue crystallography: coming of age. J. Synchrotron Rad. *6*, 891–917.

Richardson, J.S., and Richardson, D.C. (1988). Amino acid preferences for specific locations at the ends of alpha helices. Science *240*, 1648–1652.

Rubinstenn, G., Vuister, G.W., Mulder, F.A., Dux, P.E., Boelens, R., Hellingwerf, K.J., and Kaptein, R. (1998). Structural and dynamic changes of photoactive yellow protein during its photocycle in solution. Nat. Struct. Biol. *5*, 568–570.

Schlichting, I., and Chu, K. (2000). Trapping intermediates in the crystal: ligand binding to myoglobin. Curr. Opin. Struct. Biol. *10*, 744–752.

Schmidt, M., Pahl, R., Srajer, V., Anderson, S., Ren, Z., Ihee, H., Rajagopal, S., and Moffat, K. (2004). Protein kinetics: structures of intermediates and reaction mechanism from time-resolved X-ray data. Proc. Natl. Acad. Sci. USA *101*, 4799–4804.

Schmidt, M., Rajagopal, S., Ren, Z., and Moffat, K. (2003). Application of singular value decomposition to the analysis of time-resolved macromolecular x-ray data. Biophys. J. *84*, 2112–2129.

Schotte, F., Lim, M., Jackson, T.A., Smirnov, A.V., Soman, J., Olson, J.S., Phillips, G.N., Jr., Wulff, M., and Anfinrud, P.A. (2003). Watching a protein as it functions with 150-ps time-resolved x-ray crystallography. Science *300*, 1944–1947.

Sheldrick, G.M., and Schneider, T.R. (1997). SHELXL: high-resolution refinement. Methods Enzymol. *277*, 319–343.

Sprenger, W.W., Hoff, W.D., Armitage, J.P., and Hellingwerf, K.J. (1993). The eubacterium *Ectothiorhodospira halophila* is negatively phototactic, with a wavelength dependence that fits the absorption spectrum of the photoactive yellow protein. J. Bacteriol. *175*, 3096–3104.

Taylor, B.L., and Zhulin, I.B. (1999). PAS domains: internal sensors of oxygen, redox potential, and light. Microbiol. Mol. Biol. Rev. *63*, 479–506.

Terwilliger, T.C., and Berendzen, J. (1995). Difference refinement-obtaining differences between 2 related structures. Acta Crystallogr. D Biol. Crystallogr. *51*, 609–618.

Unno, M., Kumauchi, M., Hamada, N., Tokunaga, F., and Yamauchi, S. (2004). Resonance Raman evidence for two conformations involved in the L intermediate of photoactive yellow protein. J. Biol. Chem. *279*, 23855–23858.

Vaguine, A.A., Richelle, J., and Wodak, S.J. (1999). SFCHECK: a unified set of procedures for evaluating the quality of macromolecular structure-factor data and their agreement with the atomic model. Acta Crystallogr. D Biol. Crystallogr. *55*, 191–205.

van der Horst, M.A., van Stokkum, I.H., Crielaard, W., and Hellingwerf, K.J. (2001). The role of the N-terminal domain of photoactive yellow protein in the transient partial unfolding during signalling state formation. FEBS Lett. *497*, 26–30.

van Stokkum, I.H., Larsen, D.S., and van Grondelle, R. (2004). Global and target analysis of time-resolved spectra. Biochim. Biophys. Acta *1657*, 82–104.

Xie, A., Kelemen, L., Hendriks, J., White, B.J., Hellingwerf, K.J., and Hoff, W.D. (2001). Formation of a new buried charge drives a large-amplitude protein quake in photoreceptor activation. Biochemistry *40*, 1510–1517.

Accession Numbers

The refined structures have been deposited in the Protein Data Bank under accession codes 1T18, 1T19, 1T1A, 1T1B, and 1T1C for intermediates IE1, IE2, IL1, IL2, and IL3, respectively.